

RESEARCH ARTICLE | APRIL 04 2024

Structure and phase transitions in niobium and tantalum derived nanoscale transition metal perovskites, $\text{Ba}(\text{Ti},\text{M}^{\text{V}})\text{O}_3$, $\text{M}=\text{Nb},\text{Ta}$

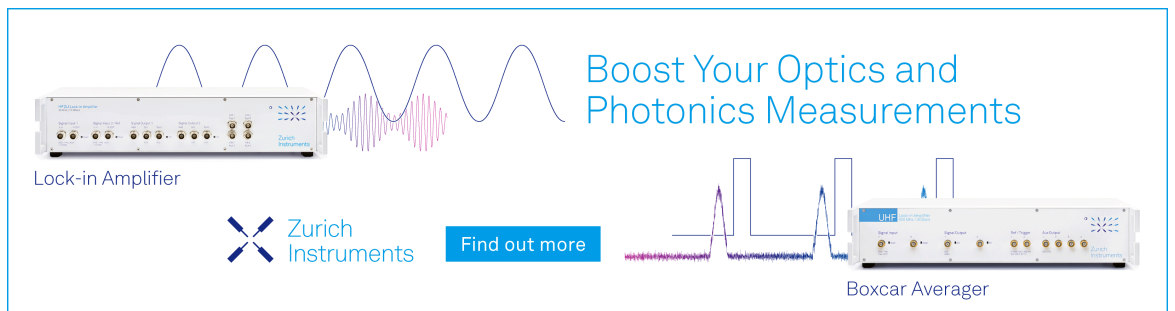
Special Collection: [Festschrift in honor of Louis E. Brus](#)

Julien Lombardi ; Long Yang ; Nasim Farahmand ; Anthony Ruffino ; Ali Younes ; Jonathan E. Spanier ; Simon J. L. Billinge ; Stephen O'Brien  



J. Chem. Phys. 160, 134702 (2024)

<https://doi.org/10.1063/5.0192488>



Boost Your Optics and Photonics Measurements

Lock-in Amplifier

 Zurich Instruments

[Find out more](#)

Boxcar Averager

Structure and phase transitions in niobium and tantalum derived nanoscale transition metal perovskites, $\text{Ba}(\text{Ti}, \text{M}^{\text{V}})\text{O}_3$, $\text{M}=\text{Nb}, \text{Ta}$

Cite as: J. Chem. Phys. 160, 134702 (2024); doi: 10.1063/5.0192488

Submitted: 19 December 2023 • Accepted: 19 February 2024 •

Published Online: 4 April 2024



View Online



Export Citation



CrossMark

Julien Lombardi,^{1,2,3} Long Yang,⁴ Nasim Farahmand,^{1,2,3} Anthony Ruffino,⁵ Ali Younes,⁶
Jonathan E. Spanier,^{5,7} Simon J. L. Billinge,⁸ and Stephen O'Brien^{1,2,3,a)}

AFFILIATIONS

¹The CUNY Energy Institute, City University of New York, Steinman Hall, 160 Convent Avenue, The City College of New York, New York, New York 10031, USA

²Department of Chemistry and Biochemistry, The City College of New York, 1024 Marshak, 160 Convent Avenue, New York, New York 10031, USA

³Ph.D. Program in Chemistry, The Graduate Center, The City University of New York, New York, New York 10016, USA

⁴School of Materials Science and Engineering, Tongji University, 4800 Caoan Road, Shanghai 201804, China

⁵Department of Physics, Drexel University, Philadelphia, Pennsylvania 19104, USA

⁶Department of Chemistry, Hunter College of the City University of New York, 695 Park Ave., New York, New York 10065, USA

⁷Department of Mechanical Engineering and Mechanics, Drexel University, Philadelphia, Pennsylvania 19104, USA

⁸Department of Applied Physics and Applied Mathematics, Columbia University, 500 West 120th Street, New York, New York 10027, USA

Note: This paper is part of the JCP Festschrift in honor of Louis E. Brus.

a) Author to whom correspondence should be addressed: sobrien@ccny.cuny.edu

ABSTRACT

The prospect of creating ferroelectric or high permittivity nanomaterials provides motivation for investigating complex transition metal oxides of the form $\text{Ba}(\text{Ti}, \text{M}^{\text{V}})\text{O}_3$, where $\text{M} = \text{Nb}$ or Ta . Solid state processing typically produces mixtures of crystalline phases, rarely beyond minimally doped Nb/Ta. Using a modified sol-gel method, we prepared single phase nanocrystals of $\text{Ba}(\text{Ti}, \text{M})\text{O}_3$. Compositional and elemental analysis puts the empirical formulas close to $\text{BaTi}_{0.5}\text{Nb}_{0.5}\text{O}_{3-\delta}$ and $\text{BaTi}_{0.5}\text{Ta}_{0.5}\text{O}_{3-\delta}$. For both materials, a reversible temperature dependent phase transition (non-centrosymmetric to symmetric) is observed in the Raman spectrum in the region 533–583 K (260–310 °C); for $\text{Ba}(\text{Ti}, \text{Nb})\text{O}_3$, the onset is at 543 K (270 °C); and for $\text{Ba}(\text{Ti}, \text{Ta})\text{O}_3$, the onset is at 533 K (260 °C), which are comparable with 390–393 K (117–120 °C) for bulk BaTiO_3 . The crystal structure was resolved by examination of the powder x-ray diffraction and atomic pair distribution function (PDF) analysis of synchrotron total scattering data. It was postulated whether the structure adopted at the nanoscale was single or double perovskite. Double perovskites ($\text{A}_2\text{B}'\text{B}''\text{O}_6$) are characterized by the type and extent of cation ordering, which gives rise to higher symmetry crystal structures. PDF analysis was used to examine all likely candidate structures and to look for evidence of higher symmetry. The feasible phase space that evolves includes the ordered double perovskite structure $\text{Ba}_2(\text{Ti}, \text{M}^{\text{V}})\text{O}_6$ ($\text{M} = \text{Nb}, \text{Ta}$) $Fm-3m$, a disordered cubic structure, as a suitable high temperature analog, $\text{Ba}(\text{Ti}, \text{M}^{\text{V}})\text{O}_3$ $Pm-3m$, and an orthorhombic $\text{Ba}(\text{Ti}, \text{M}^{\text{V}})\text{O}_3$ $Amm2$, a room temperature structure that presents an unusually high level of lattice displacement, possibly due to octahedral tilting, and indication of a highly polarized crystal.

Published under an exclusive license by AIP Publishing. <https://doi.org/10.1063/5.0192488>

PREFACE

Dear Louis, on behalf of the authors, we wish you a very Happy 80th Birthday. Some years ago, you and some of your colleagues posed the question as to whether barium titanate, BaTiO_3 , could be synthesized as nanoparticles with uniform and variable sizes. The scientific question to be answered was what happened to the ferroelectric behavior in nanocrystals as a function of size. Many years and papers later, the answer to the first question appears to be, yes, it is possible to make nanocrystals of BaTiO_3 and, indeed, other perovskites.^{1–7} In addition, the answer to the scientific question appears to be that, while atomic distortions giving rise to polarization are retained, the ferroelectric behavior is (not surprisingly) quite diminished and not as stable^{7–11} (please excuse the non-exhaustive set of references). The quest continues then, for nanoparticles that might exhibit even more pronounced remnant polarization, for future technological applications, and for stimulating yet more intellectual inquiry regarding these fascinating materials. We are grateful for your contributions to this field and for your overall exemplary leadership in nanoscale materials research.

INTRODUCTION

Synthetic nanochemistry can offer a pathway to the preparation of metastable states that represent a divergence from the true thermodynamic equilibrium, providing novel compounds of significant interest, which exhibit distinctive electronic or chemical behavior, and demonstrating an expanded range of compositions or structures previously thought to be unobtainable. In the case of complex metal oxides, using nanoscale synthetic techniques to target metastable phases can circumnavigate the large amounts of initial bond breaking associated with the oxide/carbonate precursors used in traditional solid state or ceramic processing, arriving at novel, stable compounds under ambient conditions.^{12–17} The approach can essentially situate the material in a local thermodynamic minimum under specific constraints (e.g., temperature, pressure, solvation environment, and chemical doping) that can be quenched, enabling kinetic trapping of metastable atomic configurations.^{18–22} We posited as to whether double perovskites can be made at the nanoscale, because exploring compositional options is potentially more extensive than the bulk. Exploring novel synthetic approaches to perovskite oxides continues to excite: the wide range of structural and compositional variations encompassed by the perovskite family causes it to be widely researched as a source of materials with combined dielectric, electronic, and magnetic properties.^{23–27} Structural characterization at the nanoscale often requires additional techniques and modeling due to the physical lack of long-range crystallographic order.

Ordered transition metal double perovskites comprise a large group of fascinating materials based on the formula $\text{A}_2\text{MM}'\text{O}_6$.^{28,29} The wide range of interesting properties stems from the exceptional structural and compositional flexibility.^{30–32} Recently, a class of Nb-based barium double perovskites of the form $\text{Ba}_2\text{MnNbO}_6$ ($M(3d) = \text{Sc}, \text{Ti}, \text{V}, \text{and Cr}$) have been postulated for theoretical analysis.²⁸ These hypothetical compounds are intriguing for magnetic/spintronic applications: self-consistent full-potential linear muffin-tin orbital (FP-LMTO) calculations predict $\text{Ba}_2\text{TiNbO}_6$ to be half-metallic ferromagnetic in the ground state. We targeted

synthesis of nanoscale Ba–Ti–Nb–O and Ba–Ti–Ta–O, the goal being to attempt to make nanoscale double perovskite versions of these compounds, which has proven elusive in the past when relying solely on traditional solid-state synthesis. The systems were of particular interest in the context of their theoretically calculated ferroic properties,³³ potential for magnetodielectric response, and use in devices.

In the $\text{Ba}(\text{Ti}, \text{M}^V)\text{O}_3$ system, the ideal double perovskite represents the aristotype: $\text{Ba}_2\text{TiNbO}_6$ and $\text{Ba}_2\text{TiTaO}_6$ presumed upon $Fm-3m$ transition metal sublattice order, whereas $\text{Ba}(\text{Ti}, \text{M}^V)\text{O}_3$ ($M = \text{Nb}, \text{Ta}$) might adopt a number of lower symmetries (hettotypes). Cation disorder and octahedral tilting account for deviations to a lower symmetry and have been well documented by expert crystallography in solid state chemistry.³⁴ Using a molecularly driven sol-gel synthesis approach in anhydrous polar organic solvents,³⁵ we can influence the adoption of certain cations onto the B-site.³⁶ This pathway can introduce electronic complexity into the system and alter the band structure, based upon the occupation and intermixing of the p/d-orbitals in the formation of t_{1u} , t_{2g} , t_{1g} , and t_{2g}^* molecular orbitals.^{23,37} While the structure and stoichiometry nominally dictate an $\text{A}^{2+}/\text{B}^{4+}/3\text{O}^{2-}$ formula, aliovalency at the B site can be accommodated through cation charge balancing, oxygen vacancies, and defects. This is, in theory, easier to obtain at the nanoscale, which can support a larger number of undercoordinated sites. However, the introduction of differently sized, differently charged B-site ions that interfere with charge neutrality can induce reorganization of the underlying structure, leading to the observation of perovskite-like structures with differing levels of order/disorder. Here, we ask, and attempt to answer, the question on whether double perovskites of $\text{Ba}(\text{Ti}, \text{M}^V)\text{O}_3$ can be synthesized at the nanoscale.

EXPERIMENTAL

Synthesis

Nanocrystalline samples of $\text{Ba}(\text{Ti}, \text{Nb})\text{O}_3$ (BTNO) and $\text{Ba}(\text{Ti}, \text{Ta})\text{O}_3$ (BTTO) were synthesized using a hydrothermal, sol-gel hybrid synthesis known to our group as gel collection. Barium metal 99.5% was purchased from Alfa Aesar; $\text{Ti}(\text{OCH}_2(\text{CH}_3)_2)_4$ 99.99%, $\text{Ta}(\text{OCH}_2\text{CH}_3)_5$ 99.95%, and $\text{Nb}(\text{OCH}_2\text{CH}_3)_5$ 99.95% were purchased from Sigma Aldrich; and 200 proof ethanol was purchased from Decon Laboratories Inc. All chemicals were used as purchased without further purification. The initial part of the synthesis was performed under an inert nitrogen atmosphere in a glovebox. Ba metal was dissolved in 200 proof ethanol to make a 6 wt. % solution. 1.68 mmol of the Ba solution was placed in a beaker with 0.25 ml (0.84 mmol) of $\text{Ti}(\text{OCH}_2(\text{CH}_3)_2)_4$ and 0.21 ml (0.84 mmol) of $\text{Nb}(\text{OCH}_2\text{CH}_3)_5$ or 0.22 ml (0.84 mmol) $\text{Ta}(\text{OCH}_2\text{CH}_3)_5$ (depending on whether BTNO or BTTO) and magnetically stirred for 20 min. A solution of 0.5 ml H_2O and 5 ml 200 proof ethanol was prepared and then added in 0.5 ml additions to the magnetically stirred solution. The clear yellow solution became slightly cloudy and was stirred for an additional 5 minutes. The solution was transferred to a 50 ml centrifuge tube and capped and left in the glovebox overnight (12 h) to begin the aging process. The next day, the solution was more viscous as it had begun to form a gel-like network. The solution was then transferred to a 50 ml Teflon lined stainless steel autoclave. The autoclave was sealed and heated to 200 °C

for 48 h without stirring. A nanocrystalline white gel rod formed at the bottom of the solution containing 100% of the nanocrystal products. The gel rod was easily separated from the mother solution by pouring off the excess ethanol. It was then washed three times with ethanol and water. The gel rod was then dried overnight under vacuum at 100 °C to produce a white nanocrystalline powder. Alternatively, the gel (prior to drying) can be suspended in 200 proof ethanol for up to 48 h. ICP-OES was performed on the obtained powders of BTNO and BTTO, following a sulfuric acid/nitric acid digestion procedure relying on Optima grade acids (ultra-tracer metals) and the Perkin Elmer Optima 7300 DV (Hunter College, CUNY). Based upon the data and reliability of the digestion process, a Ti/Nb ratio of 0.97 ± 0.5 and a Ti/Ta ratio of 1.09 ± 0.1 were obtained.

Characterization

The nanocrystalline powders were characterized using powder x-ray diffraction (XRD), synchrotron x-ray pair distribution function (PDF) analysis, Raman spectroscopy, transmission electron microscopy (TEM), energy-dispersive x-ray spectroscopy (EDS), and x-ray photoelectron spectroscopy (XPS). The XRD measurements of the dried BTNO powders were performed on a PANalytical X'Pert pro (Cu K α radiation). XPS measurements were recorded on the BTNO powder samples on a Physical Electronics Versaprobe II XPS. The XPS peaks were fitted using the MultiPak, version 9.6.0.15, software. Samples for the TEM were prepared by dispersing the nanocrystalline powders in 200 proof ethanol and placing 5 μ l of the resulting solution on a carbon coated copper TEM grid. TEM and EDS measurements were recorded on a JEOL 2100 microscope.

Raman spectroscopy was performed in a backscatter configuration, utilizing a linearly polarized 532 nm laser diode excitation source focused on a spot size $\sim 10 \mu$ m in diameter. Scattered light was dispersed using a micro-Raman spectrometer (Horiba Jobin-Yvon XploRa One), light below 100 cm^{-1} was filtered out, and the remainder was collected using an air-cooled CCD detector. Samples were housed in a heating stage (Linkam THMS600) purged by high purity nitrogen gas, and temperature-dependent spectra were obtained for $T = 290 \text{ K}$ to $T = 625 \text{ K}$. Spectra were collected as three 30-second scans averaged together. Due to the ceramic-like orientation of the particles in these samples, all polarizations of Raman-scattered light were collected. It is immediately apparent from the Raman spectra that both BTTO and BTNO exist in a non-centrosymmetric structure at room temperature, reminiscent of the BaTiO₃ end member ($P4mm$).^{38,39} Room temperature Raman spectra in BTTO and BTNO (Fig. S4) show strong but broadened E(TO3) and E(LO4) modes at ~ 300 and $\sim 750 \text{ cm}^{-1}$, respectively, both strong indicators of the tetragonal phase. Significant structural distortions are not expected with a B-site replacement in this case, since the ionic radii of both Nb and Ta are nearly the same as that of Ti. The higher energy broad formations in the A1(LO3)+E(LO4) mode can be attributed to the changes in the deformability of the BO₆ octahedra due to the substitution of Ti with Nb or Ta. In addition, the A1 mode at low energies are broadened by these substitutions as they represent the motion of the Ba sublattice against the BO₆ octahedra, with the increased masses lowering the frequency.^{39–42} Finally, despite sample synthesis in an inert atmosphere, exposure to ambient air when moving from synthesis to the experimental

chamber caused the formation of BaCO₃, as evidenced by the spectral features at ~ 150 and $\sim 1050 \text{ cm}^{-1}$.^{43,44} Temperature dependent Raman spectra (Fig. 4) highlight the non-centrosymmetric (tetragonal/orthorhombic) to cubic phase transition in BTTO and BTNO. Spectra were collected at 10 K increments, allowing 1 minute for the sample to equilibrate at each temperature before collection. The phase transition occurs at $\sim 550 \text{ K}$ in BTNO and $\sim 540 \text{ K}$ in BTTO, compared to $\sim 390 \text{ K}$ in BaTiO₃.^{45,46} The spectra remaining at high temperatures can be attributed to defects (~ 250 and $\sim 500 \text{ cm}^{-1}$ band)^{38,40} and remnant local disorder ($\sim 800 \text{ cm}^{-1}$),⁴⁷ of which both are seen in similar off-stoichiometry systems with ceramic-like disordering.

Determining the precise structure of crystalline nanoscale compounds can prove difficult, due to the Scherrer broadening of the Bragg peaks in the powder diffraction pattern. This can be attributed to a consequence of atomic disorder, especially at the crystallite surface, the limitation of the crystallite size in providing coherent scattering, and also, to some extent, the instrument configuration (slits, x-ray intensity, etc.). We applied pair distribution function (PDF) analysis, examining all likely candidate structures based upon the perovskite crystal group. PDF provides a level of certainty in structural elucidation that exceeds basic powder XRD diffractometers and powder spectrum analysis for local structures of nanocrystalline materials. The x-ray total scattering measurements on the BTNO and BTTO samples were carried out at the XPD beamline (28-ID-2) of the National Synchrotron Light Source II (NSLS-II), Brookhaven National Laboratory. Multiple batches of BTNO and BTTO were prepared and measured. Some samples were also heated to calcination temperatures to test the thermal stability of the compounds and to ascertain any differences in the total scattering following thermal treatment. The nanocrystalline powders were sealed in 1 mm diameter polyimide capillaries, and the data were collected at room temperature using the rapid acquisition PDF (RAPDF) method.⁴⁸ The experimental setup was calibrated by measuring the crystalline nickel as a standard material. A large area 2D PerkinElmer detector was mounted behind the samples with a sample-to-detector distance of 203.39 mm. The incident x-ray wavelength was $\lambda = 0.1901 \text{ \AA}$. The instrument resolution is explained by two parameters in modeling, Q_{damp} and Q_{broad} ,^{49,50} which were determined as $Q_{damp} = 0.038 \text{ \AA}^{-1}$ and $Q_{broad} = 0.012 \text{ \AA}^{-1}$ by fitting the PDF from a well crystallized sample of Ni. The detector exposure time was 0.1 s for all the samples to avoid detector saturation, and the number of frames taken for the sample was adjusted to be 600 for sufficient counting statistics on the data, so the total exposure time per sample was 60 s. The collected data frames were summed, corrected for polarization effects, and masked to remove outlier pixels before being integrated along arcs of constant Q , where $Q = 4\pi \sin \theta / \lambda$ is the magnitude of the momentum transfer on scattering, to produce 1D powder diffraction patterns using the PyFAI program.⁵¹ Standardized corrections and normalizations were then applied to the data to obtain the total scattering structure function, $F(Q)$, which was Fourier transformed to obtain the PDF, using PDFgetX3⁵² within xPDFsuite.⁵³ The maximum range of data used in the Fourier transform was chosen to be $Q_{max} = 23.0 \text{ \AA}^{-1}$ so as to give the best trade-off between statistical noise and real-space resolution. For consistency, all PDFs were transformed with the same settings. The PDF modeling program PDFgui was used for structure refinements. In these refinements, $Uiso (\text{Å}^2)$ is the isotropic atomic displacement parameter (ADP),

and in multiphase fits, the ADPs of the same type of atoms are constrained to be the same in different phases; $\delta 1$ (Å) is a parameter that describes correlated atomic motions;⁵⁴ and SPD (Å) is a parameter that accounts for the finite size of the particle, or more correctly, the domain of coherent scattering in the particle, which gives the diameter of the domain in angstrom units, assuming it to be spherical. Q_{damp} and Q_{broad} were refined to a nickel dataset collected under the same experimental conditions and then fixed in the nanoparticle refinements.

RESULTS AND DISCUSSION

We had set out to determine whether the nanoscale offered the possibility of developing new phase space, substitutional capability and cation ordering in oxide perovskites of Ba–Ti–(Nb/Ta)–O. The (1:1) M-cation ordered transition-metal double perovskites cover a vast range of crystalline inorganic solid-state compounds. Some effort has been made both experimentally and computationally to explore the substitutional capability and transition metal solubility for the chemical formula $A_2M'M''O_6$ but tending toward systems demonstrating substantive properties of interest. The A-site is well documented for A = Ca, Sr, Ba, La, and Nd.^{30,55} In addition, frequently, $M'M''$ sites can be exchanged with $M' = \text{Cr, Fe, Co, and Zr}$ and $M'' = \text{Mo, Re, W, and Os}$.^{56–58} The compounds include magnetoresistive varieties of $\text{Sr}_2\text{FeMoO}_6$ ³¹ and Ba_2MMoO_6 (M = Fe, Co, and Mn),⁵⁹ which are also attractive for solid oxide fuel cell research and spintronics.^{26,60} The presence of oxygen vacancies is considered critical when understanding the electrochemical and electronic behavior.⁶¹ In the case of $A_2M'M''O_6$ or $A(M', M'')O_3$, where A = Ba and $M' = \text{Ti}$, there is limited reporting on $M'' = \text{Nb or Ta}$, not least because the reasonable assumption has been that M' would be a better fit as a 3+ ion, such as La or Y.³⁰

Physical characterization

Two single phase nanomaterials were prepared based upon $\text{Ba}(\text{Ti}, \text{M}^V)\text{O}_3$, where M = niobium (Nb) or tantalum (Ta), referred to as BTNO and BTTO, respectively. Nanocrystal powders can be produced from solvothermal treatment. Size and morphology, as well as the elemental composition of the samples, were studied through the use of a JEOL 2100 TEM equipped with an EDS probe (see Fig. 1). All samples were observed to be nanocrystalline powders. The particle size distribution is observed with average particle sizes of ~20 nm and a range of 10–50 nm. The nanocrystals are considered to be fully crystallized: all samples are polycrystalline as shown by the selected area electron diffraction (SAED). While some aggregation of the particles is observed, the particles can be stably suspended in 200 proof ethanol for up to 1–2 days with sufficient sonication. An initial powder x-ray diffraction allowed a preliminary investigation of the underlying crystal structure. The recorded XRD powder patterns of the BTNO and BTTO nanopowders [Fig. 1(e)] show a primary phase resembling a primitive cubic perovskite of the $Fm\bar{3}m$ space group, common for double perovskites, such as Ba_2YTaO_6 and $\text{Sr}_2\text{FeMoO}_6$.^{62,63} If one is to suppose the double perovskite unit cell and index the reflections accordingly, a good match is given, with lattice parameter $a = 8.03$ Å for BTNO from the cubic symmetry [Fig. 1(a)], in reasonable agreement with Saad *et al.*'s prediction of the lattice parameter $a = 8.052$ Å, using an all-electron

full potential linear muffin-tin orbital (FP-LMTO) computational method.²⁸ As expected, this lattice parameter is nearly double that of cubic BaTiO_3 (BTO), 4.033 Å,⁶⁴ and by DFT calculations and measurements on nanocrystals of BaTiO_3 , such as those verified by Rabuffetti *et al.*,⁶⁵ it was found to be 4.01 Å. A lattice parameter twice the size of a cubic perovskite derivative is consistent with the classification of an ordered mixed transition metal double perovskite. This is due to the rock salt ordering of the B and B' site transition metals being part of the same unit cell. A slight shoulder on the 220 peak is observed and is indicative of minor $\text{BaCO}_{3(s)}$ impurity formed on the surface of the nanoparticles under ambient conditions presumed to be following synthesis. The observation of some BaCO_3 is expected when analyzing high surface area Ba-based perovskite titanates under atmospheric conditions, due to the reaction of atmospheric moisture/ CO_2 with surface Ba atoms. The use of purified, carbonate-free H_2O in the synthesis is necessary for this reason. Residual carbonate can also be removed by washing with purified water or acidified water, making this impurity removable from samples that show some accumulation, and avoidable if the samples are handled under moisture/ CO_2 -free conditions. Energy dispersive spectroscopy (EDS) data prove the presence of the expected elements, distributed evenly across sample sections [Figs. 1(g) and 1(h)]. Together with the ICP-EOS data, the ratios of Ti/Nb and Ti/Ta were concluded to be 1:1 within error margins. Compositional and elemental analysis puts the compound empirical formula at $\text{BaTi}_{0.5}\text{M}_{0.5}\text{O}_{3-\delta}$.

Advanced structural characterization of BTNO and BTTO: Pair distribution function analysis

While a preliminary assignment of space group and atomic organization of the nanoscale $\text{Ba}(\text{Ti}, \text{M}^V)\text{O}_3$ was possible from TEM/XRD alone, the precise structure of these novel crystalline nanoscale compounds is difficult to pinpoint, due to the Scherrer broadening of the Bragg peaks in the powder diffraction pattern. Crystal building and powder XRD simulations allow for an overview (excellent resources, such as VESTA,⁶⁶ are available for three-dimensional visualization and structural analysis) and illustrate how, for nanoscale crystalline materials, basic laboratory powder XRD is often insufficient in the discernment of the correct space group and structure. Some proposed structures and simulated powder patterns together with the raw data (see Fig. S1 of the supplementary material) show how similar structures typical for known perovskites cannot be ruled out. We applied room temperature Pair Distribution Function (PDF) analysis^{49,67–69} to examine likely candidate structures based upon the perovskite crystal group. PDF is an excellent way to resolve structure at the nanoscale while taking into account exact particle diameters when performing structural refinements for a specific space group, symmetry, and site occupancy. We sought to examine the crystalline nature of both BTNO and BTTO samples and determine site occupancy of both Nb and Ta within the crystalline lattice. PDF analysis was performed instead of Rietveld or Le Bail analysis for obtaining structural parameters since it is better suited for determining short range order within a crystal for nanoscale ordering.^{49,68–70} In addition, we utilized an auto data mining algorithm to robustly show local off-centering in long-range cubic perovskite materials.⁷¹

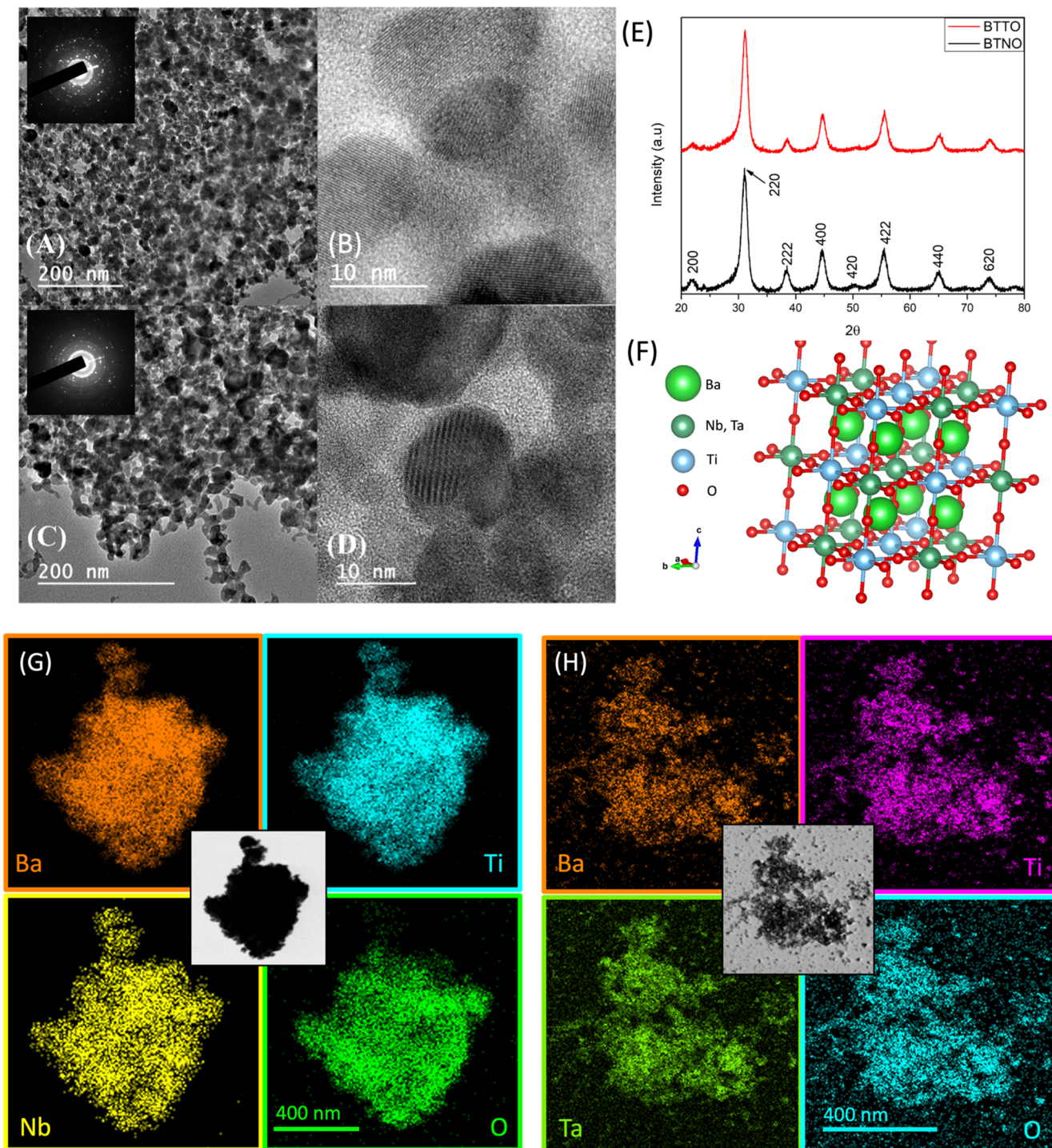


FIG. 1. Structural characterization of nanocrystalline $\text{Ba}(\text{Ti}, \text{M}^{\text{V}})\text{O}_3$, where $\text{M} = \text{niobium (Nb), "BTNO," or tantalum (Ta), "BTTO." (a) BTNO, low mag TEM with SAED, (b) high mag showing lattice images of nanocrystals, (c) BTTO, low mag TEM image with SAED, (d) high mag showing lattice images of nanocrystals, (e) indexed XRD powder diffraction patterns of BTNO and BTTO, (f) model of an ordered double perovskite cubic structure, (g) EDS of BTNO, and (h) EDS of BTTO. Scale bars for (g) and (h) are shown in the oxygen box.$

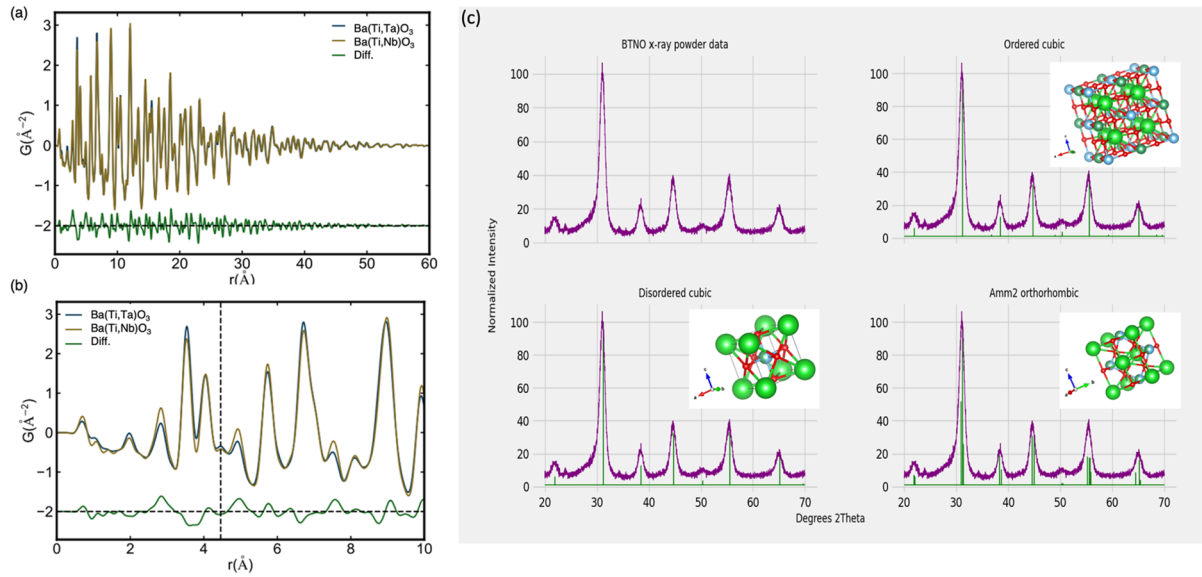


FIG. 2. X-ray PDFs of Ba(Ti,Ta)O₃ (BTTO) and Ba(Ti,Nb)O₃ (BTNO). BTTO and BTNO are superimposed with the difference curve shown beneath in green. Full-r (a) and low-r (b) regions. The two structures resemble each other very closely, due to the virtually identically observed size of VI-coordinated Nb⁵⁺ and Ta⁵⁺ ions, while the differences can be attributed to the difference in atomic form factors. (c) X-ray powder pattern of BTNO together with Vesta simulated powder patterns of perovskite lattices proposed from the PDF data, illustrating a consistent envelope of potential fits.

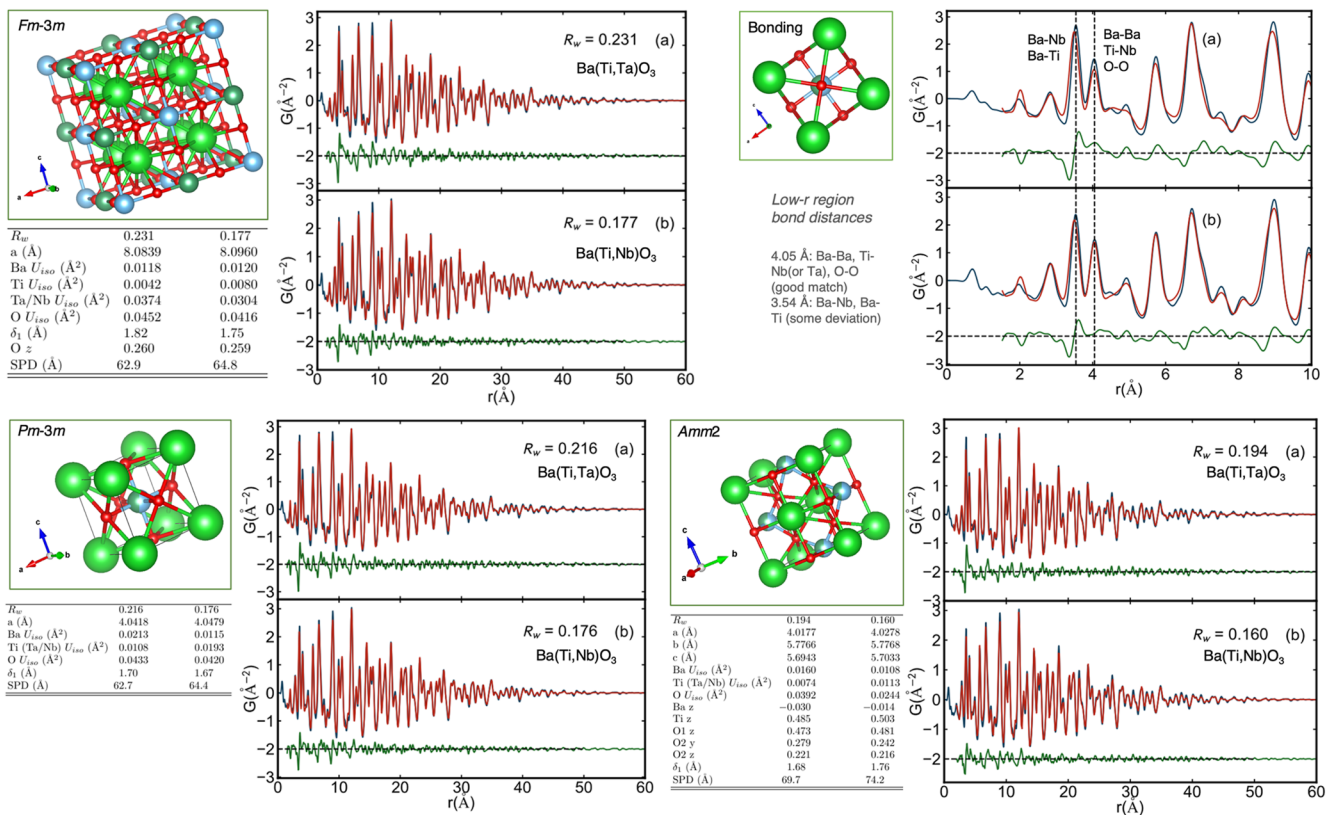


FIG. 3. X-ray PDFs of (a) BTTO and (b) BTNO fit to three OC models: ordered cubic (OC), *Fm-3m*; disordered cubic (DC), *Pm-3m*; and orthorhombic (OR), *Amm2*. Experimental PDF data are shown in blue curves, best-fit calculated PDF is shown in red, and the difference curve offset is shown beneath in green. PDF data, together with R_w values, are shown for each case. Data tables for the refinement parameters (Tables S1–S3) are provided in the supplementary material for improved readability.

TABLE I. Summary of structural models used for the PDF BTNO/BTTO fitting procedure.

Model names	OC	DC	OR
Crystal system	Ordered cubic	Disordered cubic	Orthorhombic
Centrosymmetry	Yes	Yes	No
Space group	<i>Fm-3m</i>	<i>Pm-3m</i>	<i>Amm2</i>
Ba position	(0.25, 0.25, 0.25)	(0, 0, 0)	(0, 0, 0)
Ti position	(0, 0, 0)	(0.5, 0.5, 0.5)	(0.5, 0, z)
Nb position	(0.5, 0.5, 0.5)	(0.5, 0.5, 0.5)	(0.5, 0, z)
Ta position	(0.5, 0.5, 0.5)	(0.5, 0.5, 0.5)	(0.5, 0, z)
O position	(0.254, 0, 0)	(0.5, 0.5, 0)	(0, 0, z)

The experimental PDF data are shown in Fig. 2, and analysis is shown in Fig. 3. Overall, the BTTO and BTNO samples have very similar structures and are well crystallized, as indicated by the PDF signals extending to the high- r region. Multiple batches were measured to confirm consistency, thermal stability of the samples, and reproducibility in the total scattering measurements (Fig. S2). By plotting them superimposed (Fig. 2), it can be observed that BTTO and BTNO have a very similar average and local structure, except some peak intensity difference as a consequence of the different elements present. A small shoulder at $r = 4.46$ Å is observed in the data, as indicated by the vertical dashed line [Fig. 2(b)], characteristic of a peak attributed to trace BaCO₃. Initially, three candidate perovskite models were put forward (Table I): ordered cubic (*Fm-3m*), disordered cubic (*Pm-3m*), and orthorhombic (*Amm2*), and fitted to the experimental PDFs to determine structure through refinement. The three models overall fit the PDF data well, confirming a perovskite structure. The three models were also simulated by VESTA and compared with the x-ray powder pattern of BTNO [Fig. 2(c)], illustrating that these models are also consistent, since the space group and lattice parameter derived simulations fit under the Bragg peaks. The refined spherical particle diameter (SPD) values indicate that the crystalline sizes of these nanoparticles are in the range 6–10 nm, in reasonable agreement with TEM. In all cases, the refined lattice parameters of BTTO and BTNO are close, explained by the fact that Ta(V) and Nb(V) ions with coordination VI have identical reported Shannon ionic radii of 0.64 Å.⁷²

For the ordered cubic (OC) model, the initial lattice parameters and atomic positions for fitting are $a = 8.052$ Å and oxygen at (0.254, 0, 0) and the parameters mirror that of the computational work performed by Musa Saad *et al.*²⁸ Given no published work available for tantalum or models similar to Ba₂TiTaO₆, simply replacing the Nb atom with the Ta atom was done. The initial lattice parameter for the disordered cubic (DC) model was $a = 4.026$ Å. The orthorhombic model was created with half occupancy of Ti and Nb or Ta at the B site of the perovskite with initial lattice parameters of $a = 4.0147$ Å, $b = 5.6863$ Å, and $c = 5.7141$ Å, as depicted in Fig. 3. The initial fit using the ordered cubic model (OC), shown in Fig. 2, confirms that both BTTO and BTNO samples have assumed an underlying perovskite structure. Structural refinement results are tabulated in Table S1 of the supplementary material. The OC fit of BTTO resulted in an $R_w = 0.231$, while the OC fit was marginally better for BTNO with an $R_w = 0.177$. However, the low- r difference signaled a somewhat

higher than satisfactory R_w , which prompted further modeling. This was also motivated by considerations of other acquired data, notably the Raman spectroscopy (Fig. 4), in which both BTNO and BTTO samples exhibit strong modes at room temperature (and up to 550 and 540 K in BTNO and BTTO, respectively). The Raman spectra strongly suggest polarizable phonon modes in the crystal lattice at RT, inconsistent with a centrosymmetric cubic crystal structure.

A refinement of a disordered cubic (DC) model was performed on the experimental data yielding similar results to the OC model (Fig. 3). The refinement results (Fig. 3 and Table S2 of the supplementary material) indicate the model was a close fit but show some deviation from the true crystalline structure because the Ba–Nb, Ba–Ta, and Ba–Ti distances were found to be slightly smaller to match the 3.54 Å data peak (Fig. 3). This led to the consideration of using cation displacements to improve the model. To introduce cation displacements with a non-centrosymmetric model, a refinement was performed using an orthorhombic *Amm2* space group, in which Ti and Ta/Nb occupy the same site in the perovskite structure. The refinement results (Fig. 3 and Table S3) show a noticeable improvement in R_w values in both cases, with 0.194 and 0.160 for BTTO and BTNO, respectively. The refinement coordinates indicate that the B site occupancy shared by both Ti and Nb/Ta is off-center. The data point to the existence of a possible ferroelectric phase at room temperature, due to the non-centrosymmetric nature of the crystal. Other space groups (*P4/mmm*, *P4mm*, and *R3m*) were also attempted and modeled. The results of R_w values and Ti (Nb/Ta) ADP factors, while reasonable, continue to support the theory of the *Amm2* space group (see Table S4 of the supplementary material). Finally, the degree of octahedral tilting^{73,74} was considered and modeled for these systems. While nothing conclusive was determined, some degree of Glazer tilting is certainly a possibility in these nanocrystals (see Fig. S3 of the supplementary material).

Raman spectroscopy

Raman spectroscopy was performed on powder samples of BTTO and BTNO. Initially, spectra were recorded at room temperature and subsequently heated up to around 650 K. The Raman was recorded multiple times over temperature cycles. Spectra were collected at 10 K increments, allowing 1 minute for the sample to equilibrate at each temperature before collection. The data (Fig. 4) show a reversible, temperature dependent phase transition in both BTNO and BTTO. The regions of interest in which a phase transition is concluded to occur can be readily identified. Trace BaCO₃ was also identified, and vibrational modes assigned to this phase are shown in Fig. 4. In the case of BTNO [Figs. 4(a) and 4(c)], the spectra remain the same up to 503 K, and further to 543 K. At these temperatures, vibrational modes attributed to phonon modes in the structure due to the crystal lattice can be assigned, including A₁(TO₁), 180 cm⁻¹; A₁(TO₂), 260 cm⁻¹; B₁+E(TO₃), 300 cm⁻¹; A₁(TO₃), 510 cm⁻¹; and A₁(LO₃+E(LO₄), ~720 to 850 cm⁻¹. After 543 K, the onset of a phase transition occurs, in which these modes begin to soften until 583 K at which point the peaks are significantly reduced and completion of a phase transition can be inferred. In the case of BTTO [Figs. 4(b) and 4(d)], a similar set of observations can be made for a different temperature range. From room temperature and in the range 493–533 K, a closely matching set of vibrational modes attributed to phonon modes in the structure due

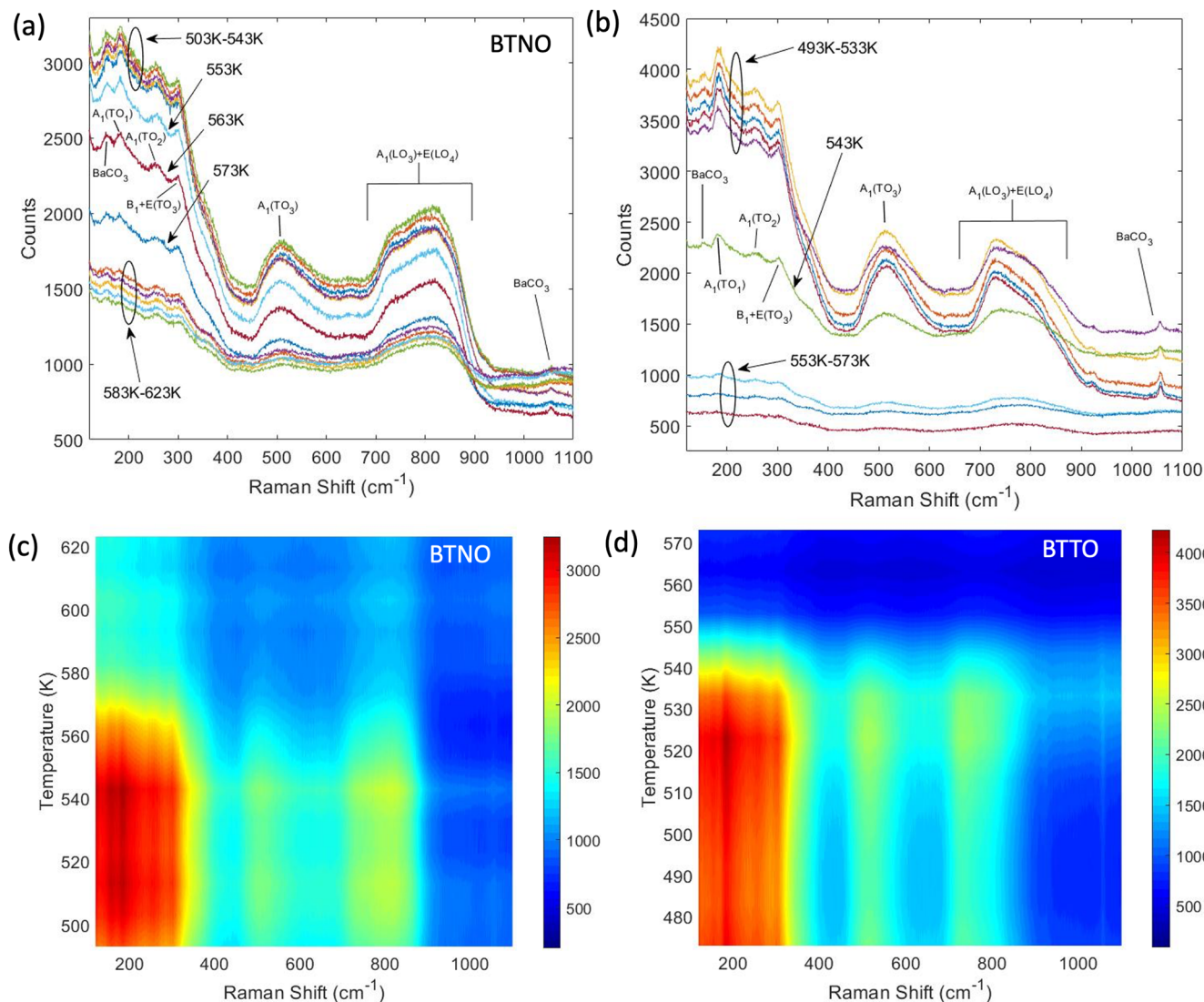


FIG. 4. (a) Temperature dependent Raman shift of BTNO with assigned modes; (b) temperature dependent Raman shift of BTTO with assigned modes; (c) temperature dependent heat map of Raman shifts in BTNO; and (d) temperature dependent heat map of Raman shifts in BTTO.

to the crystal lattice can be assigned, including $A_1(\text{TO}_1)$, 180 cm^{-1} ; $A_1(\text{TO}_2)$, 260 cm^{-1} ; $B_1+E(\text{TO}_3)$, 300 cm^{-1} ; $A_1(\text{TO}_3)$, 500 cm^{-1} ; and $A_1(\text{LO}_3)+E(\text{LO}_4)$, $\sim 710\text{ to }830\text{ cm}^{-1}$. In the case of BTTO, it is observed that an almost flat line spectrum is recorded after 553 K, strongly indicating completion of the transition.

The room temperature spectra of BTTO and BTNO (supplementary material, Fig. S4) show strong but broadened $E(\text{TO}_3)$ and $E(\text{LO}_4)$ modes at ~ 300 and $\sim 750\text{ cm}^{-1}$, respectively, strong indicators of a distortion in the lattice that would give rise to a non-centrosymmetric unit cell at RT. The observation of the completion of a phase transition at higher temperatures (583 K for BTNO; 553 K for BTTO), and mode softening to an almost flat line spectrum indicates that, at these higher temperatures, the lattice

may well become centrosymmetric, and phase transition from a distorted structure to centrosymmetric structure (e.g., $Pm\text{-}3m$) is complete. The behavior is reminiscent of BaTiO_3 ^{38,39} and suggests that both BTTO and BTNO exist in either an orthorhombic or tetragonal structure at room temperature and lower temperatures. For the Raman spectra, the difference between the tetragonal vs orthorhombic phase is hard to distinguish. PDF structural refinement gave strong evidence for the orthorhombic phase from optimized R_w and ADP values, which resulted in lattice parameters of $b = 5.7766\text{ \AA}$ and $c = 5.6943\text{ \AA}$ for BTNO and $b = 5.7768\text{ \AA}$ and $c = 5.7033\text{ \AA}$ for BTTO, while tetragonal space groups $P4/mmm$ and $P4mm$ gave comparable R_w values, but ADP less so (supplementary material, Table S4). Being that these values are close to each other

(0.0823 Å for BTTO and 0.0735 Å for BTNO), it can be concluded that Raman may also support the hypothesis of an underlying orthorhombic phase. Significant structural distortions are not expected with a B-site replacement in this case, because the ionic radii of both Nb and Ta are identical to each other ($\text{Nb}^{5+}/\text{Ta}^{5+}$, coordination VI: ionic radius 0.64 Å) and closely resemble that of Ti (Ti^{3+} , coordination VI: ionic radius 0.67 Å; Ti^{4+} , coordination VI: ionic radius 0.61 Å). The higher energy broadening in the $A_1(\text{LO}_3) + E(\text{LO}_4)$ mode can be attributed to changes in the deformability of the BO_6 octahedra due to the substitution of Ti^{4+} with Nb^{5+} or Ta^{5+} . In addition, the A_1 mode at low energies are broadened by these substitutions as they represent the motion of the Ba sublattice against the BO_6 octahedra, with the increased masses lowering the frequency.^{39–42,45,46} We can conclude, therefore, that the Raman spectra (Fig. 3) highlight the lower symmetry to cubic phase transition in BTTO and BTNO. The onset of the phase transition occurs at 543 K in BTNO and 533 K in BTTO, compared to ~ 390 K in BaTiO_3 .^{47,75} The spectra remaining at high temperatures are attributed to defects (~ 250 and ~ 500 cm^{-1} bands)^{39,42} and remnant local disorder (~ 800 cm^{-1}),⁷⁶ of which both are seen in similar

off-stoichiometry systems with ceramic-like disordering. It is interesting to contemplate that a double perovskite ordered cubic structure of the form $Fm\bar{3}m$ $\text{Ba}_2\text{TiNbO}_6$ or $\text{Ba}_2\text{TiTaO}_6$ may exist above the phase transition temperature and in the ranges 583–623 K (BTNO) and 553–573 K (BTTO), respectively.

X-ray photoelectron spectroscopy

An important problem to address in the nanocrystals of BTNO and BTTO was the determination of the likeliest valence states of the ions present. For this reason, the materials were studied by X-ray Photoelectron Spectroscopy (XPS). XPS data were recorded on a Physical Electronics Versaprobe II XPS, and the peaks were analyzed and fitted using the MultiPak, version 9.6.0.15, software. The spectra presented (Fig. 5) are from a surface analysis survey and referenced to the standard protocol C 1s-signal at 284.8 eV.⁷⁷ Additional XPS data regarding alternate fitting of Nb/Ta and the Ba and O spectra are presented in the supplementary material (Figs. S5 and S6). The Nb XPS [Fig. 5(a)] shows two peaks in the 204–212 eV region that correspond to the Nb $3d_{5/2}$ and Nb $3d_{3/2}$

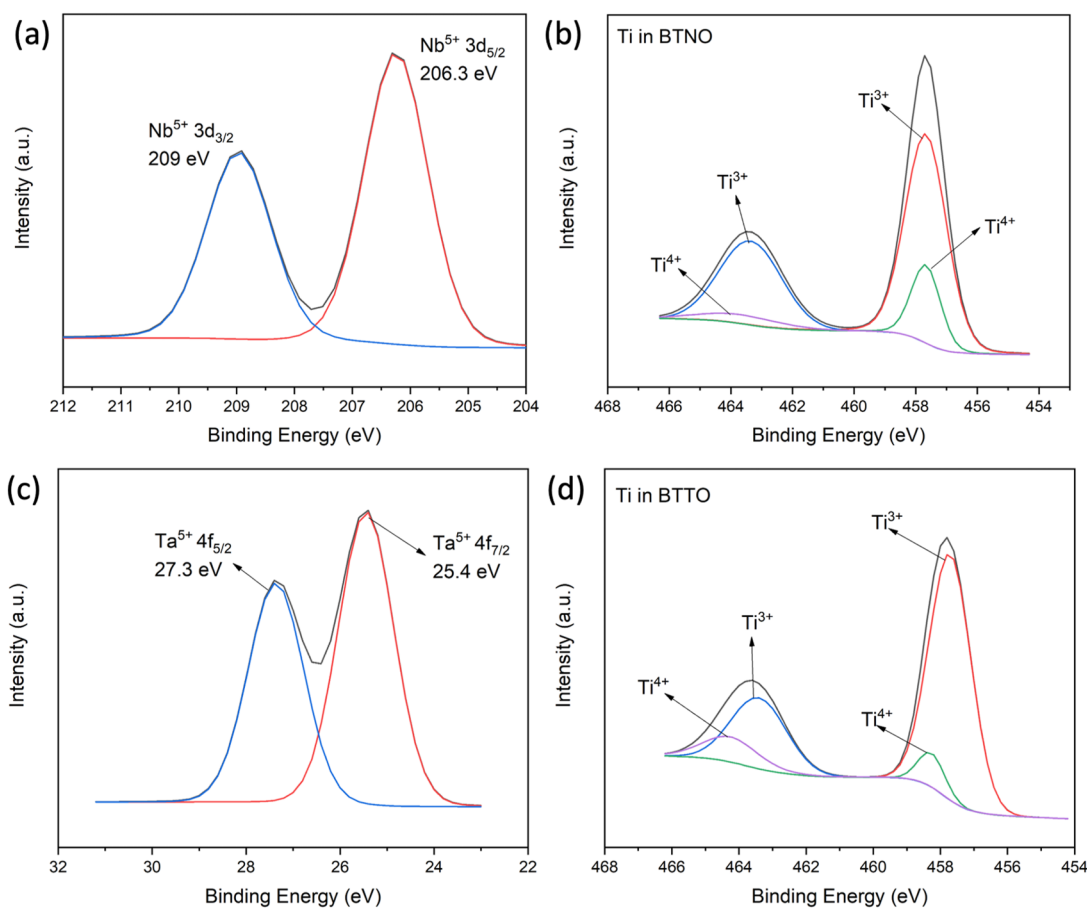


FIG. 5. X-ray photoelectron spectroscopy (XPS) of BTNO and BTTO. (a) Nb $3d_{3/2}$ and $3d_{5/2}$; (b) Ti $2p_{1/2}$ and Ti $2p_{3/2}$ in BTNO; (c) Ta $4f_{5/2}$ and $4f_{7/2}$; and (d) Ti $2p_{1/2}$ and Ti $2p_{3/2}$ in BTTO.

peaks at 209.0 and 206.3 eV, respectively. These peaks are commonly seen in the Nb₂O₅ spectra^{79,80} and is conclusive evidence that Nb⁵⁺ is incorporated into the perovskite structure, with the concurrent consideration that only one crystalline phase is observed in the x-ray diffraction pattern in Fig. 2. In the Ta XPS [Fig. 5(c)], there are two peaks that were readily identified to be the Ta 4f_{7/2} and Ta 4f_{5/2} peaks in the 22–30 eV region. The peak positions were 25.4 and 27.3 eV, respectively, and correspond to Ta⁵⁺, which is to be expected and is in good agreement with the literature reported values.⁸⁰ Similarly, this is conclusive evidence that Ta⁵⁺ is incorporated into the perovskite structure for BTTO, with the concurrent consideration that only one crystalline phase is observed in the x-ray diffraction pattern in Fig. 2. From the XPS, strong evidence is provided that both metals, niobium and tantalum, were present in the (V) oxidation state. We tested this hypothesis further by posing the question as to whether additional oxidation states might be present and how that would affect the XPS fitting in Multipak. In particular, we postulated whether Nb or Ta might be present in the +4 oxidation state. Fitting of the XPS data using some portion of Nb (IV) or Ta (IV) coupled with Nb (V) or Ta (V) was attempted (Fig. S5). The fits are unsatisfactory compared to fitting solely with Nb(V) or Ta(V). The conclusion was that Nb or Ta is present in these nanomaterials as predominantly the +5 oxidation state. However, this would also lead to the conclusion that, for charge neutrality, titanium must be coexisting in predominantly the +3 oxidation state. The presence of some oxygen vacancies, common for perovskites could compensate for the existence of some Ti^{IV} ions while still allowing for charge neutrality. The existence of Ti³⁺ in complex metal perovskite oxides is commonplace, for example in YTiO₃ and LaTiO₃.^{81,82} In our recent report on the synthesis and characterization of Eu_{0.5}Ba_{0.5}TiO₃, including XPS analysis, we provide an in-depth discussion of XPS characterization and simulation of titanium according to the proposed existence of certain oxidation states.⁸³ The XPS of titanium in these compounds show the profiles of the Ti 2p_{1/2} and Ti 2p_{3/2} in BTNO [Fig. 5(c)] and in BTTO [Fig. 5(d)]. The Ti 2p_{1/2} and Ti 2p_{3/2} spin-orbital splitting photoelectrons for both samples are located at binding energies of 463.5 and 457.7 eV, respectively, consistent with previously observed data.⁸³ Multipak fitting supported the observed predominance of Ti³⁺ in both cases combined with the presence of some Ti⁴⁺.

The barium XPS was also recorded (supplementary material, Fig. S6). A broad peak in the 777–783 eV region and a broad Ba 3d_{5/2} line were observed and fit to two peaks at 778.95 and 779.75 eV, respectively. This fitting agrees well with other BaTiO₃ solids of similar size and morphology.^{84,85} The Ba 3d_{5/2} peak has been deconvoluted into two peaks showing the bulk and surface species of Ba²⁺. Because these are nanoparticles, there is a significantly high ratio of surface/bulk Ba, evident in the XPS from the 779.75 eV peak. In the XPS of O (Fig. S6), the O 1s peak was observed in the 526–536 eV region of the spectrum. A well-defined peak at 529.75 eV was observed, characteristic of metal oxide phase, with a shoulder at 531.35 eV, which is characteristic of a metal carbonate phase. A shoulder is also observed on the 220 peak in the XRD pattern in Fig. 2, indicating the presence of BaCO₃, which this shoulder in the XPS confirms. The O 1s peak was fit similarly to the BTNO XPS; however, it was observed that the shoulder at 531.5 eV was lower in intensity, indicating that less BaCO₃ is formed in the BTTO sample than in the BTNO sample.

In conclusion, XPS data provide compelling evidence that Nb and Ta are present in Ba(Ti,M^V)O₃ (M = Nb/Ta) in predominantly the +5 formal oxidation state, with subsequent implications regarding the formal oxidation state and coordination of Ti, and potential oxygen vacancies. Further XANES characterization combined with DFT studies seeded by the structural models would serve as suitable future work to more closely examine the electronic structure implications of these conclusions.

CONCLUSION

Using a modified sol-gel method, we were able to prepare single phase nanocrystals of the form Ba(Ti, M)O₃ (M = Nb, Ta). BaTi_{0.5}Nb_{0.5}O₃ was called BTNO, and BaTi_{0.5}Ta_{0.5}O₃ was called BTTO. We conducted a thorough investigation into the structure of nanoscale BTNO and BTTO through x-ray powder diffraction, electron microscopy, elemental analysis, and pair distribution function analysis. Previous computational calculations had postulated a double perovskite structure, incorporated into our analysis. Double perovskites (A₂B'B''O₆) are characterized by the type and extent of cation ordering, which give rise to higher symmetry crystal structures. XPS data provide compelling evidence that Nb and Ta are present in Ba(Ti, M^V)O₃ (M = Nb/Ta) in predominantly the +5 formal oxidation state, with subsequent implications regarding the formal oxidation state and coordination of Ti. Raman spectroscopy shows a clear, reversible phase transition from non-centrosymmetric to symmetric, with an onset of this transition occurring at 543 K for BTNO and 533 K for BTTO. The crystal structure was resolved by examination of the powder XRD and Pair Distribution Analysis (PDF) of synchrotron data. PDF analysis was used to examine all likely candidate structures and to look for evidence of a higher symmetry. The feasible phase space that evolves includes the ordered double perovskite structure Ba₂(Ti, M^V)O₆ (M = Nb, Ta) *Fm-3m*, a disordered cubic structure, as a suitable high temperature analog, Ba(Ti, M^V)O₃ *Pm-3m*, and an orthorhombic Ba(Ti, M^V)O₃ *Amm2*, a room temperature structure that presents an unusually high level of lattice displacement, possibly due to octahedral tilting, and indication of a highly polarized crystal. This article focusses on the synthesis, structural, and spectroscopic characterization of the Ba(Ti, M^V)O₃ (M = Nb/Ta) system, with electrical characterization to be released in a sequel report in the future.

SUPPLEMENTARY MATERIAL

See the supplementary material for a comparison of postulated candidate structures for Ba(Ti,Nb)O₃: XRD diffraction patterns were compared with XRD simulations performed using VESTA (Fig. S1). Total scattering measurements (synchrotron data) of Ba(Ti,Nb)O₃ and Ba(Ti,Ta)O₃ are shown in Fig. S2: the experimental PDFs indicate consistency across samples and thermal stability. Tables S1–S4 show PDF structural refinement results of the candidate structures. Octahedral tilting was explored and is shown in Fig. S3, and single RT Raman spectra are shown in Fig. S4. Supplementary XPS data are provided in Fig. S5 and S6, together with Multipak fitting for BTNO and BTTO with included amounts of Nb⁴⁺/Ta⁴⁺ and XPS of Ba 3d_{5/2}, Ti 2p lines, Ta 4f_{5/2}, Ta 4f_{7/2} lines, and O 1s.

ACKNOWLEDGMENTS

This work was partly supported by the National Science Foundation, under NSF DMR Award No. 1461499, NSF CREST No. 2112550, and NSF DGE No. 2151945. S.O. is grateful to the PSC-CUNY Research Awards Program for additional support. S.O. and J.L. thank Dr. Ali Younes (Hunter College, CUNY) for assistance with the ICP-OES data collection. The PDF data collection, analysis, and modeling were supported as part of GENESIS: A Next Generation Synthesis Center, an Energy Frontier Research Center funded by the U.S. Department of Energy, Office of Science, Basic Energy Sciences under Award No. DE-SC0019212. X-ray PDF measurements were conducted at beamline 28-ID-2 of the National Synchrotron Light Source II, a U.S. Department of Energy (DOE) Office of Science User Facility operated for the DOE Office of Science by Brookhaven National Laboratory under Contract No. DE-SC0012704. A.J.R. and J.E.S. acknowledge support from the U.S. Army Research Office under Grant No. W911NF-21-1-0126, the U.S. Army Research Laboratory under cooperative agreement No. W911NF-19-2-0119, and the National Science Foundation under DMR 1608887.

AUTHOR DECLARATIONS

Conflict of Interest

The authors have no conflicts to disclose.

Author Contributions

Julien Lombardi (Conceptualization, Investigation, Methodology, Visualization, Writing - Original Draft): Dr. Lombardi helped conceptualize the research idea, helped define the research goals and formulating the approach to studying these nanoscale perovskites. Dr. Lombardi designed and performed the nanocrystal synthesis and conducted XRD characterization as well as participating in all other characterization. He also drafted the original manuscript. Long Yang (Investigation, Formal Analysis, Methodology, Visualization): Dr. Yang conducted synchrotron experiments and performed the PDF analysis, including data visualization, modeling, and representation. Dr. Yang co-edited the sections on PDF analysis. Nasim Farahmand (Investigation, Formal analysis, Visualization): Dr. Farahmand was responsible for XPS analysis and modeling. She also curated the XPS data, ensuring its accuracy and readiness for analysis. Anthony Ruffino (Investigation, Formal Analysis, Visualization): Dr. Ruffino was responsible for the Raman analysis, assignments, and interpretation. Dr. Ruffino acquired the temperature Raman data and contributed to the manuscript. Ali Younes (Investigation): Dr. Younes conducted the ICP-OES elemental analysis with Dr. Lombardi assisting. Jonathan Spanier (Supervision, Investigation, Methodology, Resources): Dr. Spanier contributed to the experimental investigation, oversaw, and supervised the Raman acquisition, and contributed to the intellectual content, commented on the manuscript. Simon J. L. Billinge (Supervision, Investigation, Methodology, Resources): Dr. Billinge developed the methodology for powder XRD and atomic pair distribution function analysis and supervised/contributed to the formal analysis of the synchrotron total scattering data. Dr. Billinge commented on the manuscript.

Stephen O'Brien (Project Administration, Supervision, Conceptualization, Investigation, Methodology, Data Curation, Visualization, Writing - Review & Editing, Correspondence, Funding Acquisition): As corresponding author, Dr. O'Brien helped conceptualize the research idea, helped define the research goals and formulating the approach to studying these nanoscale perovskites, secured funding for the project, performed data analysis, representation and interpretation, oversaw the writing and revision of the manuscript, and handled correspondence related to the paper.

DATA AVAILABILITY

The data that support the findings of this study are available from the corresponding author upon reasonable request.

REFERENCES

- 1 S. O'Brien, L. Brus, and C. B. Murray, "Synthesis of monodisperse nanoparticles of barium titanate: Toward a generalized strategy of oxide nanoparticle synthesis," *J. Am. Chem. Soc.* **123**(48), 12085–12086 (2001).
- 2 M. Niederberger, G. Garnweitner, N. Pinna, and M. Antonietti, "Nonaqueous and halide-free route to crystalline BaTiO₃, SrTiO₃, and (Ba,Sr)TiO₃ nanoparticles via a mechanism involving C–C bond formation," *J. Am. Chem. Soc.* **126**(29), 9120–9126 (2004).
- 3 K. Kato, K. Mimura, F. Dang, H. Imai, S. Wada, M. Osada, H. Haneda, and M. Kuwabara, "BaTiO₃ nanocube and assembly to ferroelectric supracrystals," *J. Mater. Res.* **28**(21), 2932–2945 (2013).
- 4 S. Adireddy, C. Lin, B. Cao, W. Zhou, and G. Caruntu, "Solution-based growth of monodisperse cube-like BaTiO₃ colloidal nanocrystals," *Chem. Mater.* **22**(6), 1946–1948 (2010).
- 5 F. A. Rabuffetti and R. L. Brutchey, "Structural evolution of BaTiO₃ nanocrystals synthesized at room temperature," *J. Am. Chem. Soc.* **134**(22), 9475–9487 (2012).
- 6 S. Y. Liu, L. M. Huang, W. L. Li, X. H. Liu, S. Jing, J. Li, and S. O'Brien, "Green and scalable production of colloidal perovskite nanocrystals and transparent sols by a controlled self-collection process," *Nanoscale* **7**(27), 11766–11776 (2015).
- 7 Y. Hao, Z. Feng, S. Banerjee, X. Wang, S. J. L. Billinge, J. Wang, K. Jin, K. Bi, and L. Li, "Ferroelectric state and polarization switching behaviour of ultrafine BaTiO₃ nanoparticles with large-scale size uniformity," *J. Mater. Chem. C* **9**(15), 5267–5276 (2021).
- 8 J. E. Spanier, A. M. Kolpak, J. J. Urban, I. Grinberg, L. Ouyang, W. S. Yun, A. M. Rappe, and H. Park, "Ferroelectric phase transition in individual single-crystalline BaTiO₃ nanowires," *Nano Lett.* **6**(4), 735–739 (2006).
- 9 L. Huang, Z. Chen, J. D. Wilson, S. Banerjee, R. D. Robinson, I. P. Herman, R. Laibowitz, and S. O'Brien, "Barium titanate nanocrystals and nanocrystal thin films: Synthesis, ferroelectricity, and dielectric properties," *J. Appl. Phys.* **100**(3), 1–10 (2006).
- 10 M. B. Smith, K. Page, T. Siegrist, P. L. Redmond, E. C. Walter, R. Seshadri, L. E. Brus, and M. L. Steigerwald, "Crystal structure and the paraelectric-to-ferroelectric phase transition of nanoscale BaTiO₃," *J. Am. Chem. Soc.* **130**(22), 6955–6963 (2008).
- 11 M. J. Polking, M. G. Han, A. Yourdkhani, V. Petkov, C. F. Kisielowski, V. V. Volkov, Y. Zhu, G. Caruntu, A. Paul Alivisatos, and R. Ramesh, "Ferroelectric order in individual nanometre-scale crystals," *Nat. Mater.* **11**(8), 700–709 (2012).
- 12 W. Sun, S. T. Dacek, S. P. Ong, G. Hautier, A. Jain, W. D. Richards, A. C. Gamst, K. A. Persson, and G. Ceder, "The thermodynamic scale of inorganic crystalline metastability," *Sci. Adv.* **2**(11), e1600225 (2016).
- 13 A. Navrotsky, L. Mazeina, and J. Majzlan, "Size-driven structural and thermodynamic complexity in iron oxides," *Science* **319**, 1635–1638 (2008).
- 14 A. E. Powell, J. M. Hodges, and R. E. Schaak, "Preserving both anion and cation sublattice features during a nanocrystal cation-exchange reaction: Synthesis of metastable Wurtzite-type CoS and MnS," *J. Am. Chem. Soc.* **138**(2), 471–474 (2016).

- ¹⁵R. E. Schaak and T. E. Mallouk, "Perovskites by design: A toolbox of solid-state reactions," *Chem. Mater.* **14**(4), 1455–1471 (2002).
- ¹⁶R. C. Garvie, "The occurrence of metastable tetragonal zirconia as a crystallite size effect," *J. Phys. Chem.* **69**(4), 1238–1243 (1965).
- ¹⁷N. A. Fleer, M. P. Thomas, J. L. Andrews, G. R. Waetzig, O. Gonzalez, G. W. Liu, B. S. Guiton, and S. Banerjee, "Epitaxial stabilization: Versus interdiffusion: Synthetic routes to metastable cubic HfO₂ and HfV₂O₇ from the core-shell arrangement of precursors," *Nanoscale* **11**(44), 21354–21363 (2019).
- ¹⁸A. Navrotsky, "Nanoscale effects on thermodynamics and phase equilibria in oxide systems," *ChemPhysChem* **12**(12), 2207–2215 (2011).
- ¹⁹A. J. Martinolich and J. R. Neilson, "Toward reaction-by-design: Achieving kinetic control of solid state chemistry with metathesis," *Chem. Mater.* **29**(2), 479–489 (2017).
- ²⁰A. Sclafani and J. M. Herrmann, "Comparison of the photoelectronic and photocatalytic activities of various anatase and rutile forms of titania in pure liquid organic phases and in aqueous solutions," *J. Phys. Chem.* **100**(32), 13655–13661 (1996).
- ²¹A. Parija, G. R. Waetzig, J. L. Andrews, and S. Banerjee, "Traversing energy landscapes away from equilibrium: Strategies for accessing and utilizing metastable phase space," *J. Phys. Chem. C* **122**(45), 25709–25728 (2018).
- ²²J. Gopalakrishnan, S. Uma, and V. Bhat, "Synthesis of layered perovskite oxides, ACa_{2-x}LaxNb_{3-x}Ti_xO₁₀ (A = K, Rb, Cs), and characterization of new solid acids, HCa_{2-x}LaxNb_{3-x}Ti_xO₁₀ (0 < x ≤ 2), exhibiting variable bronsted acidity," *Chem. Mater.* **5**(1), 132–136 (1993).
- ²³I. B. Bersuker, "Pseudo-Jahn-Teller effect—A two-state paradigm in formation, deformation, and transformation of molecular systems and solids," *Chem. Rev.* **113**(3), 1351–1390 (2013).
- ²⁴N. A. Spaldin, "Multiferroics: Past, present, and future," *MRS Bull.* **42**(5), 385–390 (2017).
- ²⁵A. Žužić, A. Ressler, and J. Macan, "Perovskite oxides as active materials in novel alternatives to well-known technologies: A review," *Ceram. Int.* **48**(19), Part A, 27240–27261 (2022).
- ²⁶Q. Zhang, T. Wei, and Y. H. Huang, "Electrochemical performance of double-perovskite Ba₂MMoO₆ (M=Fe, Co, Mn, Ni) anode materials for solid oxide fuel cells," *J. Power Sources* **198**, 59–65 (2012).
- ²⁷M. R. Li, P. W. Stephens, M. Croft, Z. Deng, W. Li, C. Jin, M. Retuerto, J. P. Hodges, C. E. Frank, M. Wu, D. Walker, and M. Greenblatt, "Mn₂(Fe_{0.8}Mo_{0.2})MoO₆: A double perovskite with multiple transition metal sublattice magnetic effects," *Chem. Mater.* **30**(14), 4508–4514 (2018).
- ²⁸M. Musa Saad, "The influence of the M (3d) replacement on structural, electronic and magnetic properties of Nb-based double perovskite Ba₂MNbO₆ (M = Sc, Ti, v and Cr): From FP-LMTO studies," *Comput. Mater. Sci.* **82**, 325–330 (2014).
- ²⁹D. Zając, M. Sikora, V. Prochazka, M. Borowiec, J. Stpie, C. Z. Kapusta, P. C. Riedi, C. Marquina, J. M. De Teresa, and M. R. Ibarra, "Local magnetic and electronic properties of the A₂FeM'O₆ (A = Ba, Sr, Ca, M' = Mo, Re) double perovskites," *Acta Phys. Pol., A* **111**(6), 797–820 (2007).
- ³⁰S. Vasala and M. Karppinen, "A₂B'B''O₆ perovskites: A review," *Prog. Solid State Chem.* **43**(1–2), 1–36 (2015).
- ³¹D. D. Sarma, E. V. Sampathkumaran, S. Ray, R. Nagarajan, S. Majumdar, A. Kumar, G. Nalini, and T. N. GuruRow, "Magnetoresistance in ordered and disordered double perovskite oxides, Sr₂FeMoO₆," *Solid State Commun.* **114**, 465–468 (2000).
- ³²M. C. Viola, M. J. Martínez-Lope, J. A. Alonso, P. Velasco, J. L. Martínez, J. C. Pedregosa, R. E. Carbonio, and M. T. Fernández-Díaz, "Induction of colossal magnetoresistance in the double perovskite Sr₂CoMoO₆," *Chem. Mater.* **14**(2), 812–818 (2002).
- ³³H. W. Eng, P. W. Barnes, B. M. Auer, and P. M. Woodward, "Investigations of the electronic structure of D0 transition metal oxides belonging to the perovskite family," *J. Solid State Chem.* **175**(1), 94–109 (2003).
- ³⁴P. W. Barnes, M. W. Lufaso, and P. M. Woodward, "Structure determination of A₂M³⁺TaO₆ and A₂M³⁺NbO₆ ordered perovskites: Octahedral tilting and pseudosymmetry," *Acta Crystallogr., Sect. B: Struct. Sci.* **62**(3), 384–396 (2006).
- ³⁵F. A. Pearsall *et al.*, "Polymer–nanocrystal nanocomposites: Device concepts in capacitors and multiferroics," in *IEEE Transactions on Nanotechnology* (IEEE, 2020), Vol. 19, pp.255–268
- ³⁶J. Lombardi, L. Yang, F. A. Pearsall, N. Farahmand, Z. Gai, S. J. L. Billinge, and S. O'Brien, "Stoichiometric control over ferroic behavior in Ba(Ti_{1-x}Fe_x)O₃ nanocrystals," *Chem. Mater.* **31**(4), 1318–1335 (2019).
- ³⁷I. B. Bersuker, "Pseudo Jahn-teller origin of perovskite multiferroics, magnetic-ferroelectric crossover, and magnetoelectric effects: The d⁰-d¹⁰ problem," *Phys. Rev. Lett.* **108**(13), 137202 (2012).
- ³⁸J. L. Parsons and L. Rimai, "Raman spectrum of BaTiO₃," *Solid State Commun.* **5**(5), 423–427 (1967).
- ³⁹A. Wei, L. Tian-Hui, W. Chun-Hai, D. Chuan-Ling, L. Neng-Neng, L. Yong, Q. Ze-Ming, S. Tao, W. Yu-Yin, J. Huan, T. Guang-Shan, and J. Xi-Ping, "Assignment for vibrational spectra of BaTiO₃ ferroelectric ceramic based on the first-principles calculation," *Acta Phys.-Chim. Sin.* **31**(6), 1059–1068 (2015).
- ⁴⁰J. D. Freire and R. S. Katiyar, "Lattice dynamics of crystals with tetragonal BaTiO₃ structure," *Phys. Rev. B* **37**(4), 2074–2085 (1988).
- ⁴¹D. Zhang, Y. Zhang, and S. Yang, "Microstructure and electrical properties of tantalum doped (Ba_{0.85}Ca_{0.15})(Zr_{0.10}Ti_{0.90})O₃ ceramics," *J. Mater. Sci.: Mater. Electron.* **26**(2), 909–915 (2015).
- ⁴²R. Farhi, M. El Marssi, A. Simon, and J. Ravez, "Relaxor-like and spectroscopic properties of niobium modified barium titanate," *Eur. Phys. J. B* **18**(4), 605–610 (2000).
- ⁴³Y. Shiratori, C. Pithan, J. Dornseiffer, and R. Waser, "Raman scattering studies on nanocrystalline BaTiO₃ Part I—Isolated particles and aggregates," *J. Raman Spectrosc.* **38**(10), 1288–1299 (2007).
- ⁴⁴M. Sendova, B. D. Hosterman, R. Raud, T. Hartmann, and D. Koury, "Temperature-dependent, micro-Raman spectroscopic study of barium titanate nanoparticles," *J. Raman Spectrosc.* **46**(1), 25–31 (2015).
- ⁴⁵G. H. Kwei, A. C. Lawson, S. J. L. Billinge, and S. W. Cheong, "Structures of the ferroelectric phases of barium titanate," *J. Phys. Chem.* **97**, 2368–2377 (1993).
- ⁴⁶B. D. Begg, K. S. Finnie, and E. R. Vance, "Raman study of the relationship between room-temperature tetragonality and the curie point of barium titanate," *J. Am. Ceram. Soc.* **79**(10), 2666–2672 (1996).
- ⁴⁷M. Kchikch and M. Maglione, "Electronic and lattice excitations in BaTiO₃:La," *J. Phys.: Condens. Matter* **6**(46), 10159–10170 (1994).
- ⁴⁸P. J. Chupas, X. Qiu, J. C. Hanson, P. L. Lee, C. P. Grey, and S. J. L. Billinge, "Rapid-acquisition pair distribution function (RA-PDF) analysis," *J. Appl. Crystallogr.* **36**(6), 1342–1347 (2003).
- ⁴⁹C. L. Farrow, S. J. L. Billinge, and S. J. L. Billinge, "Relationship between the atomic pair distribution function and small-angle scattering: Implications for modeling of nanoparticles," *Acta Crystallogr., Sect. A: Found. Crystallogr.* **65**, 232–239 (2009).
- ⁵⁰M. T. Shatnawi, *Local Structure of GeSe Glasses Around the Rigidity Percolation Threshold Using Atomic Pair Distribution Function and X-Ray Absorption Fine Structure Techniques* (Michigan State University, 2007).
- ⁵¹G. Ashiotis, A. Deschildre, Z. Nawaz, J. P. Wright, D. Karkoulis, F. E. Picca, and J. Kieffer, "The fast azimuthal integration Python library:pyFAI," *J. Appl. Crystallogr.* **48**(2), 510–519 (2015).
- ⁵²P. Juhás, T. Davis, C. L. Farrow, and S. J. L. Billinge, "PDFgetX3: A rapid and highly automatable program for processing powder diffraction data into total scattering pair distribution functions," *J. Appl. Crystallogr.* **46**(2), 560–566 (2013).
- ⁵³X. Yang, P. Juhás, C. L. Farrow, and S. J. L. Billinge, "xPDFsuite: An end-to-end software solution for high throughput pair distribution function transformation, visualization and analysis," *arXiv:1402.3163 [cond-mat.mtrl-sci]* (2015), pp. 1–4.
- ⁵⁴L.-K. Jeong, T. Proffen, F. Mohiuddin-Jacobs, and S. J. L. Billinge, "Measuring correlated atomic motion using X-ray diffraction," *J. Phys. Chem. A* **103**(7), 921–924 (1999).
- ⁵⁵M. W. Lufaso and P. M. Woodward, "Prediction of the crystal structures of perovskites using the software program SPuDS," *Acta Crystallogr., Sect. B: Struct. Sci.* **57**(6), 725–738 (2001).
- ⁵⁶A. Arulraj, K. Ramesha, J. Gopalakrishnan, and C. N. R. Rao, "Magnetoresistance in the double perovskite Sr₂CrMoO₆," *J. Solid State Chem.* **155**(1), 233–237 (2000).
- ⁵⁷K.-I. Kobayashi, T. Okuda, Y. Tomioka, T. Kimura, and Y. Tokura, "Possible percolation and magnetoresistance in ordered double perovskite alloys Sr₂Fe(W_{1-x}Mo_x)O₆," *J. Magn. Magn. Mater.* **218**(1), 17–24 (2000).

- ⁵⁸L. Fuoco, D. Rodriguez, T. Peppel, and P. A. Maggard, "Molten-salt-mediated syntheses of $\text{Sr}_2\text{FeReO}_6$, $\text{Ba}_2\text{FeReO}_6$, and $\text{Sr}_2\text{CrReO}_6$: Particle sizes, B/B' site disorder, and magnetic properties," *Chem. Mater.* **23**(24), 5409–5414 (2011).
- ⁵⁹Y.-H. Huang, G. Liang, M. Croft, M. Lehtimäki, M. Karppinen, and J. B. Goodenough, "Double-perovskite anode materials Sr_2MMoO_6 (M = Co, Ni) for solid oxide fuel cells," *Chem. Mater.* **21**(11), 2319–2326 (2009).
- ⁶⁰Q. Tang and X. Zhu, "Half-metallic double perovskite oxides: Recent developments and future perspectives," *J. Mater. Chem. C* **10**(41), 15301–15338 (2022).
- ⁶¹D. Stoeffler and S. Colis, "Ab initio study of the electronic structure of $\text{Sr}_2\text{FeMoO}_6$ double perovskites presenting oxygen vacancies or/and antisite imperfections," *Mater. Sci. Eng.: B* **126**(2-3), 133–138 (2006).
- ⁶²W. Li, L. Ning, and P. A. Tanner, "Double perovskite structure: A vibrational and luminescence investigation providing a perspective on crystal field strength," *J. Phys. Chem. A* **116**(27), 7337–7344 (2012).
- ⁶³T. Yamamoto, J. Liiimatainen, J. Linden, M. Karppinen, and H. Yamauchi, "Novel methods of synthesis and wet-chemical redox analysis for magneto-resistant double-perovskite $\text{Sr}_2\text{FeMoO}_{6-w}$," *J. Mater. Chem.* **10**(10), 2342–2345 (2000).
- ⁶⁴Q. Zhang, T. Cagin, and W. A. Goddard, "The ferroelectric and cubic phases in BaTiO_3 ferroelectrics are also antiferroelectric," *Proc. Natl. Acad. Sci. U. S. A.* **103**(40), 14695–14700 (2006).
- ⁶⁵Z. Sun, L. Zhang, F. Dang, Y. Liu, Z. Fei, Q. Shao, H. Lin, J. Guo, L. Xiang, N. Yerra, and Z. Guo, "Experimental and simulation-based understanding of morphology controlled barium titanate nanoparticles under co-adsorption of surfactants," *CrystEngComm* **19**(24), 3288–3298 (2017).
- ⁶⁶K. Momma and F. Izumi, "Vesta: A three-dimensional visualization system for electronic and structural analysis," *J. Appl. Crystallogr.* **41**(3), 653–658 (2008).
- ⁶⁷T. Egam and S. J. L. Billinge, *Underneath the Bragg Peaks: Structural Analysis of Complex Materials*, 2nd ed. (Elsevier, Amsterdam, 2012).
- ⁶⁸P. Juhás, C. L. Farrow, X. Yang, K. R. Knox, and S. J. L. Billinge, "Complex modeling: A strategy and software program for combining multiple information sources to solve ill posed structure and nanostructure inverse problems," *Acta Crystallogr., Sect. A: Found. Adv.* **71**, 562–568 (2015).
- ⁶⁹S. J. L. Billinge and I. Levin, "The problem with determining atomic structure at the nanoscale," *Science* **316**(5824), 561–565 (2007).
- ⁷⁰S. J. L. Billinge and M. G. Kanatzidis, "Beyond crystallography: The study of disorder, nanocrystallinity and crystallographically challenged materials with pair distribution functions," *Chem. Commun.* **2004**, 749–760.
- ⁷¹L. Yang, P. Juhás, M. W. Terban, M. G. Tucker, and S. J. L. Billinge, "Structure-Mining: Screening structure models by automated fitting to the atomic pair distribution function over large numbers of models," *Acta Crystallogr., Sect. A: Found. Adv.* **76**(3), 395–409 (2020).
- ⁷²R. D. Shannon, "Revised effective ionic radii and systematic studies of interatomic distances in halides and chalcogenides," *Acta Crystallogr., Sect. A* **32**, 751–767 (1976).
- ⁷³A. M. Glazer, "The classification of tilted octahedra in perovskites," *Acta Crystallogr., Sect. B: Struct. Crystallogr. Cryst. Chem.* **28**(11), 3384–3392 (1972).
- ⁷⁴C. J. Howard and H. T. Stokes, "Group-theoretical analysis of octahedral tilting in perovskites," *Acta Crystallogr., Sect. B: Struct. Sci.* **54**(6), 782–789 (1998).
- ⁷⁵S. Mukhopadhyay and T. Chen, "Surface chemical states of barium titanate: Influence of sample processing," *J. Mater. Res.* **10**, 1502 (1995).
- ⁷⁶Z. Guo, L. Yang, H. Qiu, X. Zhan, J. Yin, and L. Cao, "Structural, magnetic and dielectric properties of Fe-doped BaTiO_3 solids," *Mod. Phys. Lett. B* **26**(09), 1250056 (2012).
- ⁷⁷G. Greczynski and L. Hultman, "Compromising science by ignorant instrument calibration—Need to revisit half a century of published XPS data," *Angew. Chem., Int. Ed.* **59**(13), 5002–5006 (2020).
- ⁷⁸M. M. Rahman, R. A. Rani, A. Z. Sadek, A. S. Zoolfakar, M. R. Field, T. Ramireddy, K. Kalantar-Zadeh, and Y. Chen, "A vein-like nanoporous network of Nb_2O_5 with a higher lithium intercalation discharge cut-off voltage," *J. Mater. Chem. A* **1**(36), 11019–11025 (2013).
- ⁷⁹L. Kong, C. Zhang, J. Wang, W. Qiao, L. Ling, and D. Long, "Nanoarchitected Nb_2O_5 hollow, Nb_2O_5 @carbon and NbO_2 @carbon core-shell microspheres for ultrahigh-rate intercalation pseudocapacitors," *Sci. Rep.* **6**, 21177 (2015).
- ⁸⁰H. El-Sayed, S. Singh, M. T. Greiner, and P. Kruse, "Formation of highly ordered arrays of dimples on tantalum at the nanoscale," *Nano Lett.* **6**(12), 2995–2999 (2006).
- ⁸¹A. E. Bocquet, T. Mizokawa, K. Morikawa, A. Fujimori, S. R. Barman, K. Maiti, D. D. Sarma, Y. Tokura, and M. Onda, "Electronic structure of early 3d-transition-metal oxides by analysis of the 2p core-level photoemission spectra," *Phys. Rev. B* **53**(3), 1161–1170 (1996).
- ⁸²C. Yang and J. Xu, "Structural, optical and dielectric properties of non-crystalline LaTiO_3 films prepared by electron-beam evaporation," *J. Mater. Sci.: Mater. Electron.* **27**(11), 11934–11939 (2016).
- ⁸³N. Farahmand, C. K. McGinn, Q. Zhang, Z. Gai, I. Kymissis, and S. O'Brien, "Magnetic and dielectric property control in the multivalent nanoscale perovskite $\text{Eu}_{0.5}\text{Ba}_{0.5}\text{TiO}_3$," *Nanoscale* **13**(23), 10365–10384 (2021).
- ⁸⁴F. A. Pearsall, J. Lombardi, and S. O'Brien, "Monomer derived poly(furfuryl)/ BaTiO_3 0-3 nanocomposite capacitors: Maximization of the effective permittivity through control at the interface," *ACS Appl. Mater. Interfaces* **9**(46), 40324–40332 (2017).
- ⁸⁵R. Ayouchi, F. Mart, and D. Leinen, "Compositional, structural and electrical characterization of barium titanate thin films prepared on fused silica and Si (111) by spray pyrolysis," *Surface Interface Anal.* **30**, 565–569 (2000).